Int. J. Solids Structures Vol. 14, pp. 663–679

0020-7683/78/0801-0663/$02.00/0

ELEVATED TEMPERATURE INELASTIC ANALYSIS OF METALLIC MEDIA UNDER TIME VARYING LOADS USING STATE VARIABLE THEORIES

SUBRATA MUKHERJEE
Department of Theoretical and Applied Mechanics, Cornell University, Ithaca, NY 14853, U.S.A.

VIRENDRA KUMAR
Department of Materials Science and Engineering, Cornell University, Ithaca, NY 14853, U.S.A.

and

KAUNG JAIN CHANG
Rock Mechanics and Explosives Research Center, University of Missouri, Rolla, MO 65401, U.S.A.†

(*Received* 11 *October* 1977; *in revised form* 27 *February* 1978; *received for publication* 16 *March* 1978)

Abstract—A general method for analysing the time-dependent inelastic response of three-dimensional metallic bodies to arbitrary time-varying mechanical loads and temperature is presented in this paper. The method is capable of using any of a number of constitutive relations using state variables that have been recently proposed by other researchers. The constitutive equations due to Hart are used in the numerical calculations. Hart's model has been previously shown to accurately simulate the deformation behavior of uniaxial metallic specimens subjected to various histories of stress and strain. Numerical results are presented here for the mechanical response of a sphere to various prescribed internal pressure or internal displacement histories. Various experimentally observed phenomena in creep and plasticity such as constant stress creep, stress redistribution, history dependence, creep recovery, plastic work hardening, strain rate sensitivity and Bauschinger's effect are shown to be qualitatively predicted by Hart's model for this multiaxial problem.

1. INTRODUCTION

The classical theories of creep described in the books by Rabotnov[1], Penny and Marriott[2] and Odqvist[3], for example, have several drawbacks as discussed by Krempl[4–6]. To overcome shortcomings of classical theories and to have more faithful representations of the time dependent non-elastic deformation of metals and alloys at elevated temperatures, a broad class of newer constitutive relations have been proposed in recent years in terms of state variables by various researchers[7–13]. The present authors recently proposed[14–16] an efficient method for inelastic analysis of three-dimensional bodies subjected to *steady* loadings and temperature distributions, using these state variable theories. In the present paper, a general time-dependent inelastic analysis procedure for three-dimensional bodies subjected to arbitrary *time-varying* mechanical loads and temperatures, is presented. The loads are supposed to vary slowly in time so that inertia effects are negligible. A brief review of the salient features of state variable theories is presented in the next section. The reader is referred to[7–13] for a more detailed discussion. This is followed by a presentation of the computational scheme for general three-dimensional problems and then an illustrative problem involving a sphere. Numerical results are presented for the response of a 304 stainless steel sphere at 400°C to a variety of internal pressure and internal displacement histories. Hart's complete constitutive relations are used in these calculations. The significance of phenomena such as creep, stress redistribution history dependence, creep recovery, plastic work hardening, strain-rate sensitivity and Bauschinger's effect are discussed in the context of Hart's theory.

2. STATE VARIABLE THEORIES

The mathematical structure of the state variable theories of inelastic deformation[7–13] has some salient features which permit a simple and efficient method of time-dependent, three

†Formerly: Department of Theoretical and Applied Mechanics, Cornell University, Ithaca, NY 14853, U.S.A.

dimensional inelastic analysis. According to these theories, the total strain tensor ϵ at any time consists of the sum of the elastic strain ϵ^e, the nonelastic strain ϵ^n and the thermal strain ϵ^T. Thus, in terms of rates

$$\dot{\epsilon} = \dot{\epsilon}^e + \dot{\epsilon}^n + \dot{\epsilon}^T. \tag{1}$$

The nonelastic strain ϵ^n is time and history dependent and includes both the time-independent plastic (in the sense of classical plasticity) and time-dependent creep strains. There is no yield surface in the sense that ϵ^n is assumed to exist at all stages of the deformation process.

The nonelastic behavior is described in terms of certain well defined state variables $\mathbf{q}_i$ $(i = 1, \ldots n)$ which may be scalars or tensors. These state variables are assumed to completely characterize the present deformation state of the material and differentiate between geometrically identical specimens with different initial deformation states. They vary along the deformation path according to certain laws and their values at the current time depend upon the deformation history upto this time. Moreover, the history dependence of the rate of nonelastic strain upto the current time is completely taken into account by the values of $\mathbf{q}_i$ at this time and no further knowledge of the prior deformation history is required. With this in view, the constitutive equations assume the forms

$$\dot{\epsilon}^n = \mathbf{f}(\sigma, \mathbf{q}_i, T) \tag{2}$$

$$\dot{\mathbf{q}}_i = \mathbf{g}_i(\sigma, \mathbf{q}_i, T) \tag{3}$$

where σ is the stress tensor and T the temperature. Also, nonelastic deformation is assumed deviatoric, i.e.

$$\dot{\epsilon}^n_{kk} = 0. \tag{4}$$

Because of this, the stress σ in eqns (2) and (3) is often replaced by its deviatoric part defined as

$$\mathbf{s} = \sigma - (1/3)\sigma_{kk}\mathbf{I}. \tag{5}$$

In the above, a tensor A has caresian components A_{ij} and, as usual, a repeated index implies summation over that index. I is the identity tensor. The initial deformation state of the structure must be specified by prescribing initial values of the state variables $\mathbf{q}_i$.

Many of these state variable theories try to include various phenomena such as strain rate sensitivity, work-hardening, Bauschinger's effect, history dependence, creep recovery, material softening etc. that are observed in metals at elevated temperatures. The state variables $\mathbf{q}_i$ have different meanings in different theories. The proposed computational scheme depends only upon the mathematical structure of the constitutive relations as described above and not upon their explicit forms. Therefore, these specific forms are not given here. The specific forms of Hart's constitutive equations, used in numerical calculations, are presented later in the paper.

3. COMPUTATIONAL METHOD

A computational method for solving boundary value problems for three-dimensional metallic bodies subjected to time-varying loads and temperature distributions is presented below. The proposed method consists of formulating a given problem in terms of real time rates which leads to an inhomogeneous linear boundary value problem for the stress or displacement rates. The linear boundary value problem thus obtained is solved to find the rates of the variables of interest throughout the body at any time, and then these rates are integrated forward in time to obtain the time-histories of the variables of interest.

The governing differential equations of the problem in terms of rates are as follows:

kinematic:
$$\dot{\epsilon}_{ij} = \dot{\epsilon}^e_{ij} + \dot{\epsilon}^n_{ij} + \dot{\epsilon}^T_{ij} = \frac{1}{2}(\dot{u}_{i,j} + \dot{u}_{j,i}) \tag{6}$$

or, equivalently, the total strain rates must satisfy the compatibility equation

$$\nabla \times \dot{\boldsymbol{\epsilon}} \times \nabla = e_{imp} e_{jsk} \dot{\epsilon}_{ps,mk} = 0 \tag{7}$$

equilibrium:

$$\dot{\sigma}_{ij,j} = -\dot{F}_i \tag{8}$$

constitutive:

$$\dot{\epsilon}^e_{ij} = \frac{1}{2G}\left(\dot{\sigma}_{ij} - \frac{\nu}{1+\nu}\dot{\sigma}_{kk}\delta_{ij}\right) \tag{9}$$

$$\dot{\boldsymbol{\epsilon}}^n = \mathbf{f}(\boldsymbol{\sigma}, \mathbf{q}_i, T) \tag{10}$$

$$\dot{\epsilon}^T_{ij} = \alpha \dot{T} \delta_{ij} \tag{11}$$

$$\dot{\mathbf{q}}_i = \mathbf{g}_i(\boldsymbol{\sigma}, \mathbf{q}_i, T). \tag{12}$$

In the above u_i is the displacement vector, F_i the body force vector per unit volume, ν the Poisson's ratio, G the shear modulus, α the coefficient of linear thermal expansion, e_{ijk} the alternating tensor, δ_{ij} the Kronecker delta and ∇ the gradient operator.

3.1 *Stress rate formulation*

Using the constitutive eqns (6) and (9), the compatibility equation (7) becomes

$$\nabla \times \left[\frac{1}{2G}\left(\dot{\boldsymbol{\sigma}} - \frac{\nu}{1+\nu}\dot{\sigma}_{kk}\mathbf{I}\right)\right] \times \nabla = -\nabla \times \dot{\boldsymbol{\epsilon}}^n \times \nabla - \nabla \times [\alpha \dot{T}\mathbf{I}] \times \nabla. \tag{13}$$

The traction boundary condition is

$$\dot{\sigma}_{ij} n_j = \dot{\tau}_i \tag{14}$$

where $\mathbf{n}$ is the unit outward normal to the surface S of the body and τ the surface traction vector prescribed on S.

3.2 *Displacement rate formulation*

The equilibrium eqn (8), written in terms of displacement rates using eqn (6) and eqns (9) and (11), becomes

$$\dot{u}_{i,jj} + \frac{1}{1-2\nu}\dot{u}_{j,ji} = -\frac{\dot{F}_i}{G} + 2\dot{\epsilon}^n_{ij,j} + \frac{2(1+\nu)}{1-2\nu}\alpha \dot{\bar{T}}_{,i}. \tag{15}$$

The boundary conditions can either involve stresses, i.e.

$$\dot{\sigma}_{ij} n_j = G\left(\frac{2\nu}{1-2\nu}\dot{u}_{j,j}n_i + (\dot{u}_{i,j} + \dot{u}_{j,i})n_j - 2\dot{\epsilon}^n_{ij}n_j - \frac{2(1+\nu)}{1-2\nu}\alpha \dot{T} n_i\right)$$

$$= \dot{\tau}_i \text{ on } S \tag{16}$$

or displacements, i.e.

$$\dot{u}_i = \dot{\Delta} \text{ on } S \tag{17}$$

where Δ is the prescribed displacement vector on the surface of the body.

The initial conditions are obtained by specifying the initial distribution of state variables $\mathbf{q}_i(\mathbf{x}, 0)$ throughout the body, and by taking the initial nonelastic strains to be zero. Thus the total initial strain only has elastic and thermal components so that the initial stresses are given by the solution of the corresponding thermoelastic problem with identical material and geometry. Thus

$$\sigma_{ij}(\mathbf{x}, 0) = \hat{\sigma}_{ij}(\mathbf{x}), \epsilon_{ij}(\mathbf{x}, 0) = \hat{\epsilon}_{ij}(\mathbf{x}) = \epsilon^e_{ij}(\mathbf{x}, 0) + \epsilon^T_{ij}(\mathbf{x}, 0)$$

$$\epsilon^n_{ij}(\mathbf{x}, 0) = 0, q_i(\mathbf{x}, 0) = \hat{q}_i(\mathbf{x}) \tag{18}$$

where $\dot{\sigma}_{ij}$ and $\dot{\epsilon}_{ij}$ correspond to the thermoelastic solution. The thermoelastic solution always determines $\dot{\sigma}_{ij}$ and $\dot{\epsilon}_{ij}$ regardless of the magnitudes of the initial loads and state variables.

Thermomechanical coupling is ignored. The temperature on the surface of the body S is assumed to change slowly in time and thermal steady state conditions are assumed to exist throughout the body at each time. Thus, at any time, the temperature $T(\mathbf{x}, t)$ throughout the body is obtained by solving the steady state heat conduction equation subject to prescribed (time varying) thermal boundary conditions on the surface S. The body force distribution is also assumed to be completely prescribed throughout the body at all times.

The resulting boundary value problems discussed in Sections 3.1 and 3.2 are linear in stress rates and displacement rates respectively. The inhomogeneous terms on the r.h.s. of eqns (8), (13) and (15) are known at any time provided that the spatial distributions of stresses, state variables, temperature and body forces are known at that time. The structure of these boundary value problems is seen to be very similar to those of classical thermoelasticity.

4. ILLUSTRATIVE PROBLEMS

The formulation of boundary value problems involving a sphere subjected to time varying loads and temperature distributions is presented in this section.

A thick spherical shell of internal and external radii a and b is subjected to internal and external pressures $p(t)$ and $q(t)$. The internal temperature is $T_a(t)$ and the external temperature $T_b(t)$ (Fig. 1). Because of spherical symmetry, the only nonzero displacement component is the radial displacement $u(r, t)$ and the nonzero stress and strain components are σ_r, $\sigma_\theta = \sigma_\phi$, ϵ_r and $\epsilon_\theta = \epsilon_\phi$.

The kinematic and equilibrium equations have the usual forms given in Kumar and Mukherjee [15, 16]. The constitutive equations are:

$$\epsilon_r = [\sigma_r - 2\nu\sigma_\theta]/E + \epsilon_r^n + \alpha T \tag{19}$$

$$\epsilon_\theta = [(1-\nu)\sigma_\theta - \nu\sigma_r]/E + \epsilon_\theta^n + \alpha T \tag{20}$$

$$\dot{\epsilon}_r^n = f_r(\sigma, \mathbf{q}_l), \quad \dot{\epsilon}_\theta^n = f_\theta(\sigma, q_l) \tag{21}$$

$$\dot{\epsilon}_r^n + 2\dot{\epsilon}_\theta^n = 0 \tag{22}$$

In the above, E is the Young's modulus. To this list eqn (3) must be added. The boundary conditions are as given in [16] with p, q, T_a, T_b functions of time. The initial conditions are

$$\mathbf{q}_l(r, 0) = \mathbf{q}_l^0(r) \tag{23}$$

together with the zero time thermoelastic solution to the problem given in Timoshenko and Goodier [17] (see also Kumar [18]).

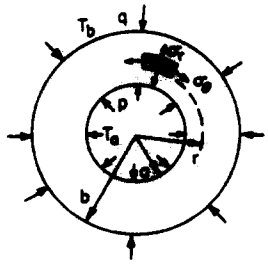

Fig. 1. Sphere under internal and external pressure.

Using the displacement rate formulation outlined in Section 3.2 the displacement rate and then the stress rates are obtained. The stress rates are given by the following equations

$$\dot{\sigma}_r = \left(\frac{E}{1-\nu}\right)\left(\int_a^r \frac{\dot{\epsilon}_r^n}{\eta}\,d\eta - \frac{(r^3-a^3)}{(b^3-a^3)}\frac{b^3}{r^3}\int_a^b \frac{\dot{\epsilon}_r^n}{\eta}\,d\eta\right) + \frac{1}{r^3(a^3-b^3)}[\dot{p}a^3(b^3-r^3) + \dot{q}b^3(r^3-a^3)]$$
$$+ \frac{\alpha E(\dot{T}_a - \dot{T}_b)ab}{(1-\nu)(b^3-a^3)}\left[a+b-\frac{(a^2+ab+b^2)}{r}+\frac{a^2b^2}{r^3}\right] \tag{24}$$

$$\dot{\sigma}_\theta = \left(\frac{E}{1-\nu}\right)\left(\int_a^r \frac{\dot{\epsilon}_r^n}{\eta}\,d\eta - \frac{(2r^3+a^3)}{2(b^3-a^3)}\frac{b^3}{r^3}\int_a^b \frac{\dot{\epsilon}_r^n}{\eta}\,d\eta + \frac{\dot{\epsilon}_r^n}{2}\right) + \frac{1}{2r^3(a^3-b^3)}[-\dot{p}a^3(2r^3+b^3)$$
$$+ \dot{q}b^3(2r^3+a^3)] + \frac{\alpha E(\dot{T}_a - \dot{T}_b)ab}{(1-\nu)(b^3-a^3)}\left[a+b-\frac{a^2+ab+b^2}{2r}-\frac{a^2b^2}{2r^3}\right] \tag{25}$$

$$\dot{T} = \dot{T}_b + (\dot{T}_a - \dot{T}_b)\frac{a}{(b-a)}\left(\frac{b}{r}-1\right). \tag{26}$$

The first term in either of eqns (24) or (25) is due to the presence of nonelastic strain rates. The second is the time derivative of Lame's elastic solution of the problem and the third is the time derivative of the thermoelastic component of the stress.

The problem can now be solved using a suitable scheme for integration in time and the time histories of the variables of interest obtained.

Another problem of interest is the response of a sphere to prescribed internal radial displacement and external pressure. The boundary conditions for this problem are

$$u(a,t) = u_a(t) \tag{27}$$

$$\sigma_r(b,t) = -q(t). \tag{28}$$

For simplicity, the temperature is assumed to be uniform throughout the sphere and steady in time. In this case, the stress rate eqns (24) and (25) must be replaced by

$$\dot{\sigma}_r = \left(\frac{E}{1-\nu}\right)\left(\int_a^r \frac{\dot{\epsilon}_r^n}{\eta}\,d\eta - \frac{f(r)}{f(b)}\frac{b^3}{r^3}\int_a^b \frac{\dot{\epsilon}_r^n}{\eta}\,d\eta\right) + \frac{2E}{f(b)}a^3\left(1-\frac{b^3}{r^3}\right)\frac{\dot{u}_a}{a} - \frac{f(r)}{f(b)}\frac{b^3}{r^3}\dot{q} \tag{29}$$

$$\dot{\sigma}_\theta = \left(\frac{E}{1-\nu}\right)\left(\int_a^r \frac{\dot{\epsilon}_r^n}{\eta}\,d\eta + \frac{\dot{\epsilon}_r^n}{2} + \frac{g(r)}{f(b)}\frac{b^3}{r^3}\int_a^b \frac{\dot{\epsilon}_r^n}{\eta}\,d\eta\right) + \frac{Ea^3}{f(b)}\left(2+\frac{b^3}{r^3}\right)\frac{\dot{u}_a}{a} + \frac{g(r)}{f(b)}\frac{b^3}{r^3}\dot{q} \tag{30}$$

where

$$f(r) = 2(1-2\nu)a^3 + (1+\nu)r^3 \tag{31}$$

$$g(r) = (1-2\nu)a^3 - (1+\nu)r^3. \tag{32}$$

5. HART'S CONSTITUTIVE RELATIONS

The constitutive relations proposed by Hart[7, 8, 19] are used in numerical calculations for the problems discussed in the previous section. Hart's equations have been used to accurately predict uniaxial deformation behavior of several metals and alloys. Recently, uniaxial creep and tensile tests were carried out on Nickel and 304 stainless steel specimens at various temperatures for various values of stress and strain rate and the results compared with predictions from Hart's constitutive equations. The correlation between theory and experiment was found to be very good. These results are available in [20] and [21]. A brief review of Hart's constitutive relations is presented in this section. The details can be obtained from [7, 8, 19].

According to Hart, the nonelastic strain rate $\dot{\epsilon}^n$ for grain matrix deformation, consists of

two components

$$\dot{\epsilon}^n = \dot{\epsilon}^a + \dot{\epsilon}^p. \tag{33}$$

Here ϵ^a is the anelastic strain due to grain matrix deformation, a stored strain that is eventually completely recoverable upon unloading, and $\dot{\epsilon}^p$ is the permanent strain rate. The corresponding permanent strain ϵ^p is path dependent and completely irrecoverable. The state variables are the anelastic strain tensor ϵ^a and scalar hardness σ^*. The path dependent nonelastic strain, ϵ^n, is explicitly rejected as a state variable. Let s represent the deviatoric part of stress tensor σ. The deviatoric stress tensor s is composed of two auxiliary tensors $\mathbf{s}^a$ and $\mathbf{s}^f$

$$\mathbf{s} = \mathbf{s}^a + \mathbf{s}^f. \tag{34}$$

The flow relations are

$$\epsilon^a = \frac{3}{2}\frac{\epsilon^a}{\sigma^a}\mathbf{s}^a \tag{35}$$

$$\dot{\epsilon}^p = \frac{3}{2}\frac{\dot{\epsilon}^p}{\sigma^a}\mathbf{s}^a \tag{36}$$

$$\dot{\epsilon}^n = \frac{3}{2}\frac{\dot{\epsilon}^n}{\sigma^f}\mathbf{s}^f \tag{37}$$

where $\dot{\epsilon}^n$, $\dot{\epsilon}^p$, ϵ^a, σ, σ^a and σ^f are scalers defined as

$$\begin{gathered}\dot{\epsilon}^n = \sqrt{\left(\frac{2}{3}\dot{\epsilon}^n_{ij}\dot{\epsilon}^n_{ij}\right)}, \quad \dot{\epsilon}^p = \sqrt{\left(\frac{2}{3}\dot{\epsilon}^p_{ij}\dot{\epsilon}^p_{ij}\right)}, \quad \epsilon^a = \sqrt{\left(\frac{2}{3}\epsilon^a_{ij}\epsilon^a_{ij}\right)} \\ \sigma = \sqrt{\left(\frac{3}{2}s_{ij}s_{ij}\right)}, \quad \sigma^a = \sqrt{\left(\frac{3}{2}s^a_{ij}s^a_{ij}\right)}, \quad \sigma^f = \sqrt{\left(\frac{3}{2}s^f_{ij}s^f_{ij}\right)}.\end{gathered} \tag{38}$$

These scalers are related to each other through the uniaxial relations

$$\sigma^a = \mathcal{M}\epsilon^a \tag{39}$$

$$\dot{\epsilon}^n = \dot{a}^*\left(\frac{\sigma^f}{\mathcal{M}}\right)^M \tag{40}$$

$$\dot{\epsilon}^p = \dot{\epsilon}^*\left(\ln\frac{\sigma^*}{\sigma^a}\right)^{-1/\lambda} \tag{41}$$

$$\dot{\sigma}^* = \dot{\epsilon}^p\sigma^*\Gamma(\sigma^*, \sigma^a) \tag{42}$$

where

$$\dot{\epsilon}^* = \left(\frac{\sigma^*}{G}\right)^m f \exp\left(-\frac{Q}{RT}\right). \tag{43}$$

In the above $\mathcal{M}$, M, m, λ, f, and $\dot{a}^*$ are flow parameters for a material and some of these are functions of temperature, R is the gas constant, Q the activation energy for atomic self-diffusion and G the shear modulus at temperature T. The work hardening function is Γ. The flow parameters are determined experimentally from a series of load relaxation and load change tests and the work hardening function from a series of strain hardening tests. It can be verified easily that the above constitutive relations have the same structure as described by eqns (2)–(4). An alternative but equivalent formulation is given in [8] where the strain invariants and flow

rules are written without numerical multipliers, e.g.

$$\dot{\epsilon}^n = \sqrt{(\dot{\epsilon}^n_{ij}\dot{\epsilon}^n_{ij})}, \quad \dot{\epsilon}^n = \frac{\dot{\epsilon}^n}{\sigma'} s^j, \quad \text{etc.}$$

In this case a set of uniaxial quantities must be suitably defined in terms of the invariants in order to ensure consistency of the uniaxial and multiaxial equations (see Table 1).

Table 1. Equivalence of 3-D and uniaxial quantities, in case of isotropy, for Hart's formulation in Ref.[8], (Similar relationships hold for other strains, strain-rates and stresses)

3-D quantities	uniaxial quantities
σ	$\sqrt{\left(\frac{2}{3}\right)}\sigma_1$
$\dot{\epsilon}^n$	$\sqrt{\left(\frac{3}{2}\right)}\dot{\epsilon}_1{}^n$
M	$\frac{2}{3}M_1$
σ^*	$\sqrt{\left(\frac{2}{3}\right)}\sigma_1{}^*$
$\dot{\epsilon}^*$	$\sqrt{\left(\frac{3}{2}\right)}\dot{\epsilon}_1{}^*$
$\dot{a}^*$	$\left(\frac{2}{3}\right)^{(M-1)/2}\dot{a}_1{}^*$
Γ	$\sqrt{\left(\frac{2}{3}\right)}\Gamma_1$

The viscoplastic limit

Hart's equations (33)–(43) can be directly used for numerical computation. However, in the region $\sigma^a \simeq \sigma^*$, eqn (41) predicts large values of $\dot{\epsilon}^p$ and consequently very small time-steps are required in the computation. For the sake of computational efficiency, the condition $\dot{\sigma}^a = \dot{\sigma}^*$ can be used to replace eqn (41) in this region. It can be shown easily that in this case the new equation for $\dot{\epsilon}^p$ becomes

$$\dot{\epsilon}^p = \frac{s^a_{ij}\dot{\epsilon}^n_{ij}/\sigma^a}{1 + \dfrac{\sigma^*\Gamma}{M}}. \tag{44}$$

The region where $\sigma^a \simeq \sigma^*$ and $\dot{\sigma}^a = \dot{\sigma}^*$ is called the viscoplastic limit. The justification for the use of the condition $\dot{\sigma}^a = \dot{\sigma}^*$ is the shape of the $\ln\sigma^a$–$\ln\dot{\epsilon}^n$ curves obtained experimentally (see for example, Figs. 5, 7 and 8 in [8]). It is observed that these curves become essentially flat (i.e. $\sigma^a \simeq \sigma^*$) for sufficiently large values of $\dot{\epsilon}^p$. Thus, the relation $\dot{\sigma}^a = \dot{\sigma}^*$ can be used whenever $\dot{\epsilon}^p$ exceeds a certain critical value $\dot{\epsilon}_c{}^p$. This critical value depends on σ^* according to the equation

$$\dot{\epsilon}_c{}^p = \dot{\epsilon}^p_{cd}(\sigma^*/\sigma_d{}^*)^m \tag{45}$$

which is a straight line in a log–log plot. Some problems might arise following sharp discontinuities in loading histories. In this case, one simply reverts back to eqn (41) instead of (44).

Equation (44) has been used instead of (41) in the viscoplastic limit region in the numerical calculations presented in the next section. This considerably improves computational efficiency without altering the results significantly. Further details regarding the viscoplastic limit are available in [20].

6. NUMERICAL RESULTS AND DISCUSSION

Results of numerical calculations carried out for a 304 stainless steel sphere at a uniform temperature of 400°C are presented in this section. The work hardening function in this case has

the form

$$\Gamma(\sigma^*, \sigma^e) = (\beta/\sigma^*)^{\delta}(\sigma^e/\sigma^*)^{\beta/\sigma^*}. \tag{46}$$

The values of the various flow parameters are [20, 21]

$$\lambda = 0.15 \qquad M = 7.8 \qquad m = 5$$

$$\dot{a}^* = 0.6937 \times 10^{25}\,\text{sec}^{-1} \qquad \mathcal{M} = 0.132 \times 10^{8}\,\text{psi}$$

$$\dot{\epsilon}^* = 0.252 \times 10^{-20}(\sigma^*/45{,}670)^5\,\text{sec}^{-1}.$$

The work hardening parameters are

$$\beta = 0.179 \times 10^{6}\,\text{psi} \qquad \delta = 1.33$$

and the parameters defining the viscoplastic limit are

$$\dot{\epsilon}_d^{pc} = 0.2123 \times 10^{-8}\,\text{sec}^{-1} \qquad \sigma_d^* = 10{,}000\,\text{psi}.$$

Finally, the elastic constants are

$$E = 0.244 \times 10^{8}\,\text{psi} \qquad \nu = 0.298.$$

In the above, the hardness and stress are in units of psi and time is in seconds.

The appropriate equations are nondimensionalized through the use of the following dimensionless variables

$$\bar{\gamma} = \gamma/\Sigma \tag{47}$$

where γ is any variable having the dimensions of stress and $\Sigma = 10{,}000$ psi. Also,

$$\xi = r/a, \quad k = b/a, \quad \bar{u} = u/a. \tag{48}$$

Either the internal pressure or the internal displacement is assumed to be prescribed in time and the external pressure q is taken to be zero for all time in all cases. The initial stresses and strains are obtained from Lame's elastic solution to the appropriate problem. The initial anelastic and permanent strains are taken to be zero in all cases while the initial hardness distribution is prescribed at an uniform value throughout the sphere.

The time rates of change of the relevant quantities at zero time are obtained from Hart's constitutive equations (33)–(43) and the stress rate equations (24) and (25) or (29) and (30). The stresses, displacements and state variables at a new time Δt are obtained using a modified Euler predictor-corrector scheme of the type

$$\frac{dy}{dt} = f(y, t) \tag{49}$$

$$y^P(t + \Delta t) = y(t) + \Delta t f(y, t) \tag{50}$$

$$y^C(t + \Delta t) = y(t) + \frac{1}{2}\Delta t(f(y, t) + f(y^P, t + \Delta t)) \tag{51}$$

$$y(t + \Delta t) = (4/5)y^C(t + \Delta t) + (1/5)y^P(t + \Delta t). \tag{52}$$

These values at time Δt are now used to find the new rates at $t = \Delta t$ and so on, and the process continued upto the final desired time. The maximum percentage difference between predictor and corrector values for any variable being integrated, at any spatial location within

the sphere, at any time step, is limited to 0.05%. A much tighter error bound does not alter the results significantly.

The radius ratio k for the sphere is 1.5 and the dimensionless shell thickness $k-1$ is divided into 20 equal segments for these numerical calculations. Spatial integrals are evaluated using Simpson's rule. Typical computing times for single calculations are between 1 and 2 min on an IBM 370/168 computer.

Numerical results for several prescribed histories of internal pressure and internal displacement are presented in Figs. 2–14. Results for constant internal pressure are shown in Figs. 2–5. It is seen from Fig. 2 that an initially hardened sphere (11% initial cold work) creeps less than an identical annealed sphere at the same pressure (15 ksi). As expected, larger pressures cause more "initial" deformation and creep and the response is highly non-linear. For a pressure of 20 ksi, for example, the hoop strain at the inner wall of the sphere is about 1.55% within a very short time. This is the sum of the elastic and "instantaneous plastic" strain of classical plasticity. Redistribution of stress invariants and hardness and of radial and tangential stress are shown in Figs. 3–5. The anelastic stress invariant σ^a, which is initially zero, increases till it equals the initial hardness (17 ksi) at the inner wall (Fig. 3). The hardness is then driven up until $\sigma^a \approx \sigma^*$ throughout the sphere. At all times, $\sigma^* \geq \sigma^a$ and $\sigma \geq \sigma^a$. The "instantaneous" deformation of classical plasticity is accumulated very quickly during the saturation of the anelastic stress invariant σ^a. Redistribution of the radial and tangential stresses (Figs. 4 and 5) is simulated as expected. A discontinuity in the slope of the tangential stress is seen to propagate quickly from the inside to the outside of the sphere.

The response to an interrupted load history is shown in Fig. 6. There is creep recovery at zero load. The effect of previous history on subsequent deformation is evident from the displacement at the inner wall of the sphere upon reloading. The material hardens and the creep rate is lower than at the start. The change of hardness and the anelastic stress invariant at the inner wall with time for this case is shown in Fig. 7. The state variables have different values at the point of reloading compared to those at the start and this causes the difference in the response of the sphere.

The response to a load change is shown in Fig. 8. The creep strain rate increases upon

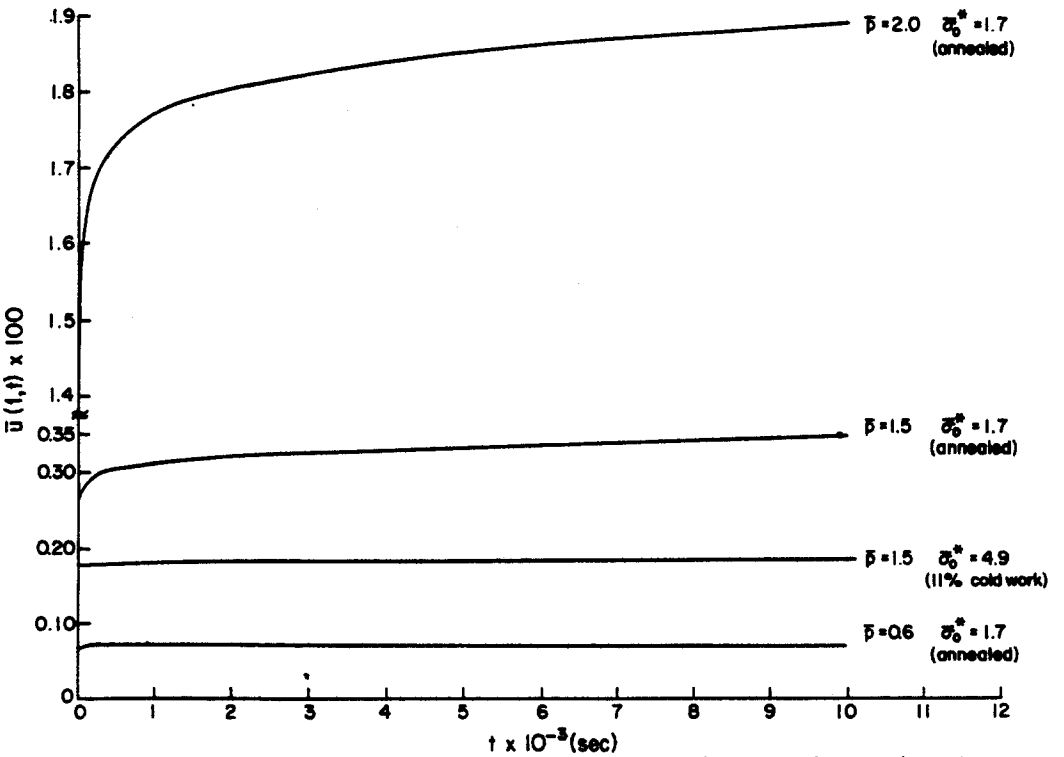

Fig. 2. Creep—radial displacements at inner wall as functions of time for various values of constant internal pressure and initial hardness.

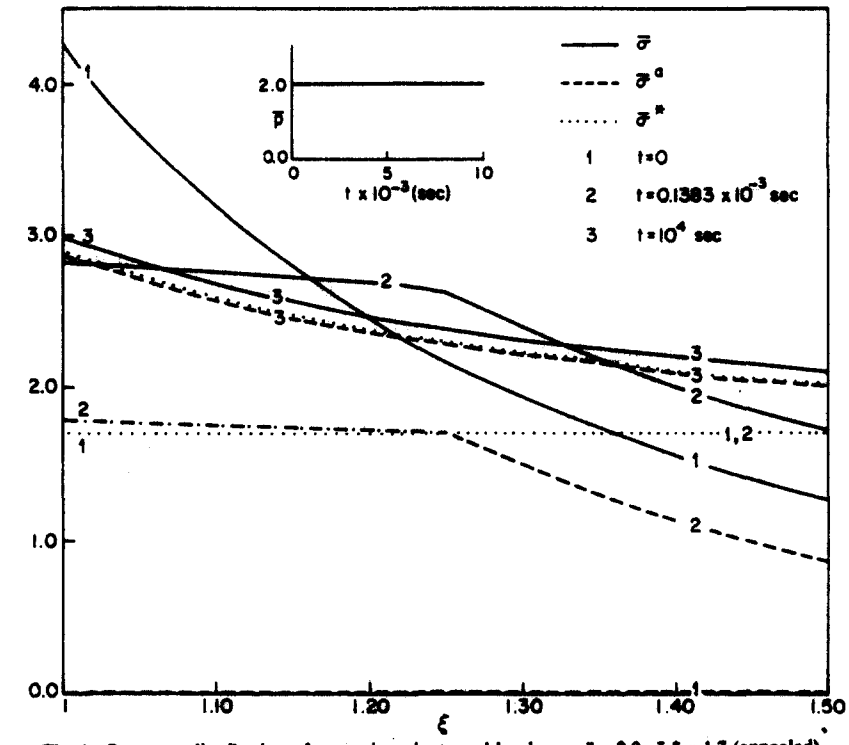

Fig. 3. Creep—redistribution of stress invariants and hardness. $\beta = 2.0$, $\bar{\sigma}_0^* = 1.7$ (annealed).

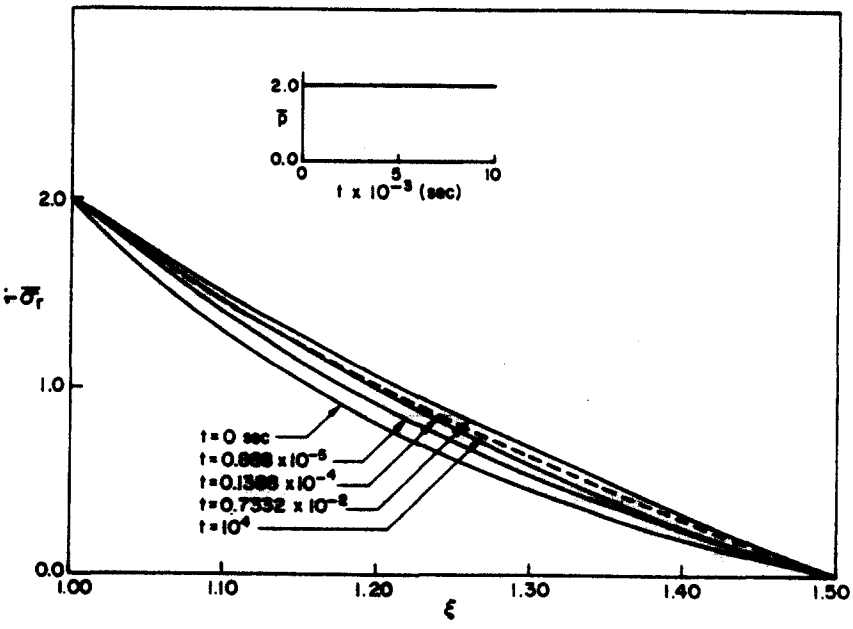

Fig. 4. Creep—redistribution of radial stress. $\beta = 2.0$, $\bar{\sigma}_0^* = 1.7$ (annealed).

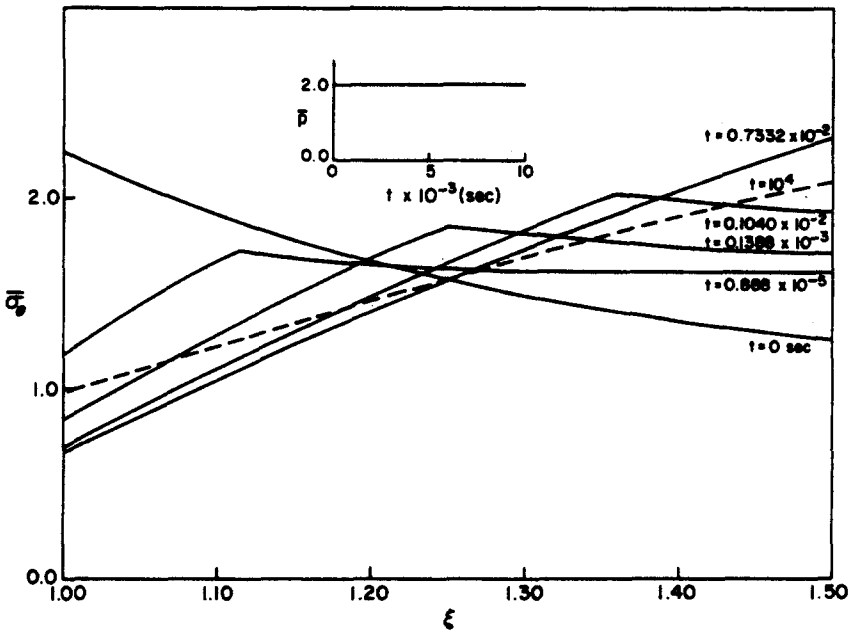

Fig. 5. Creep—redistribution of tangential stress. $\bar{p} = 2.0$, $\bar{\sigma}_0^0 = 1.7$ (annealed).

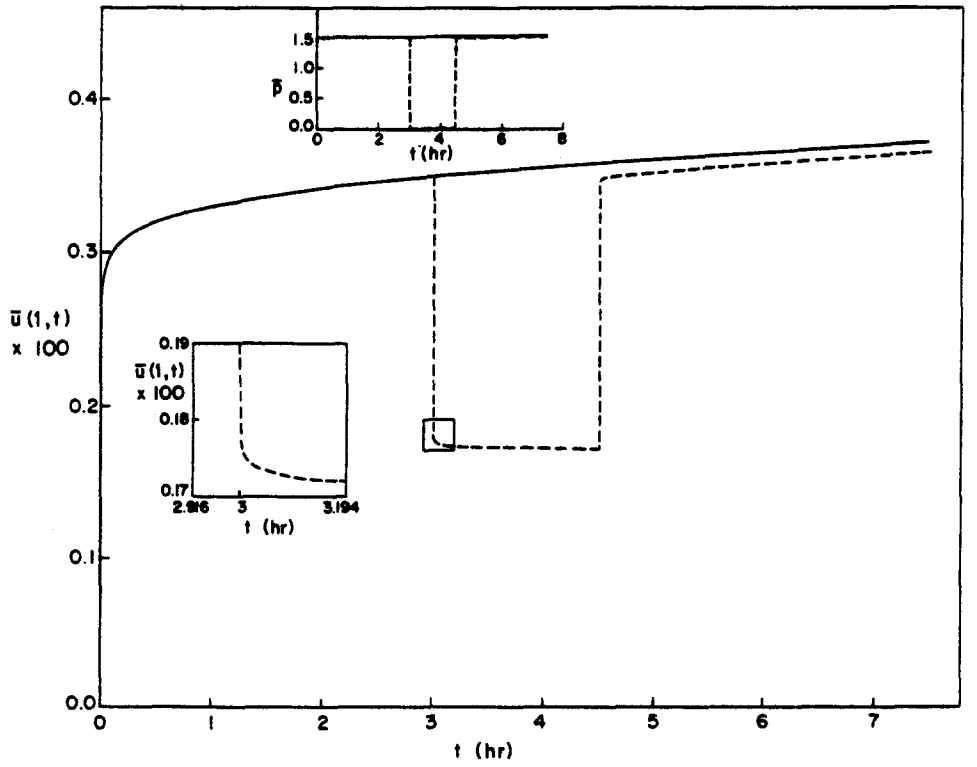

Fig. 6. Interrupted load—radial displacement at the inner wall as a function of time. $\bar{\sigma}_0^0 = 1.7$ (annealed).

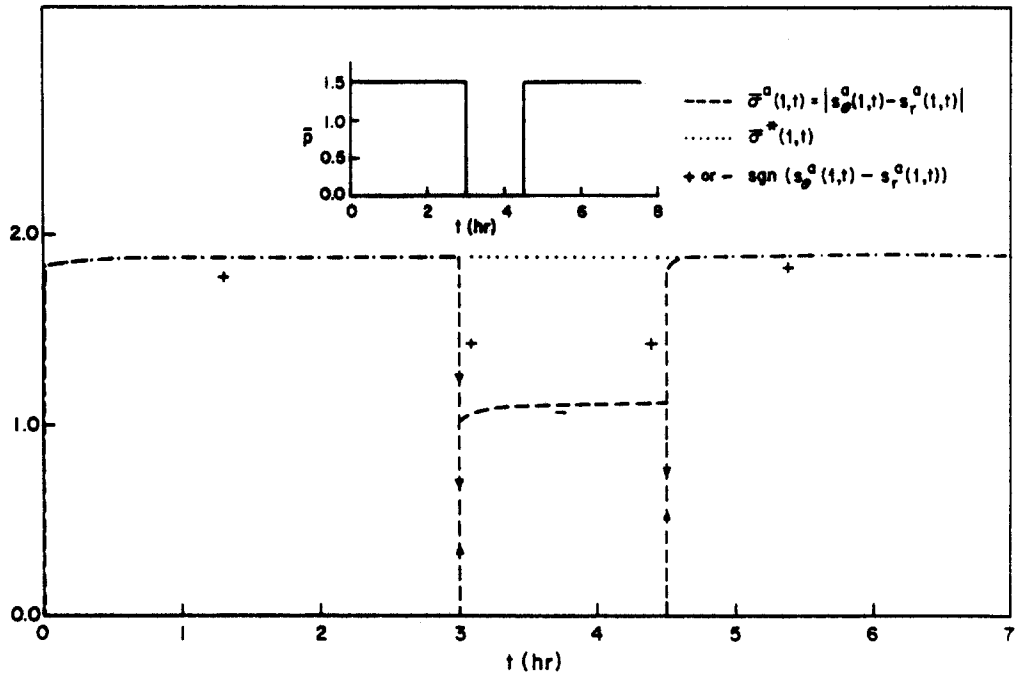

Fig. 7. Interrupted load—hardness and anelastic stress invariant at the inner wall as functions of time. $\bar{\sigma}_0^* = 1.7$ (annealed).

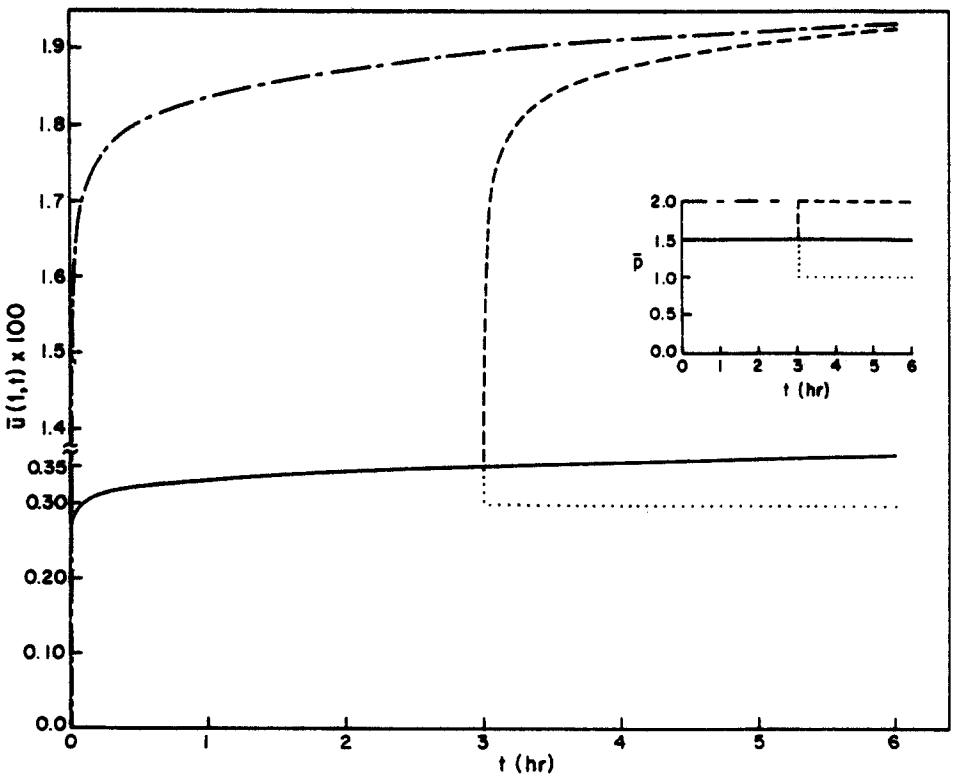

Fig. 8. Load change—radial displacement at the inner wall as a function of time. $\bar{\sigma}_0^* = 1.7$ (annealed).

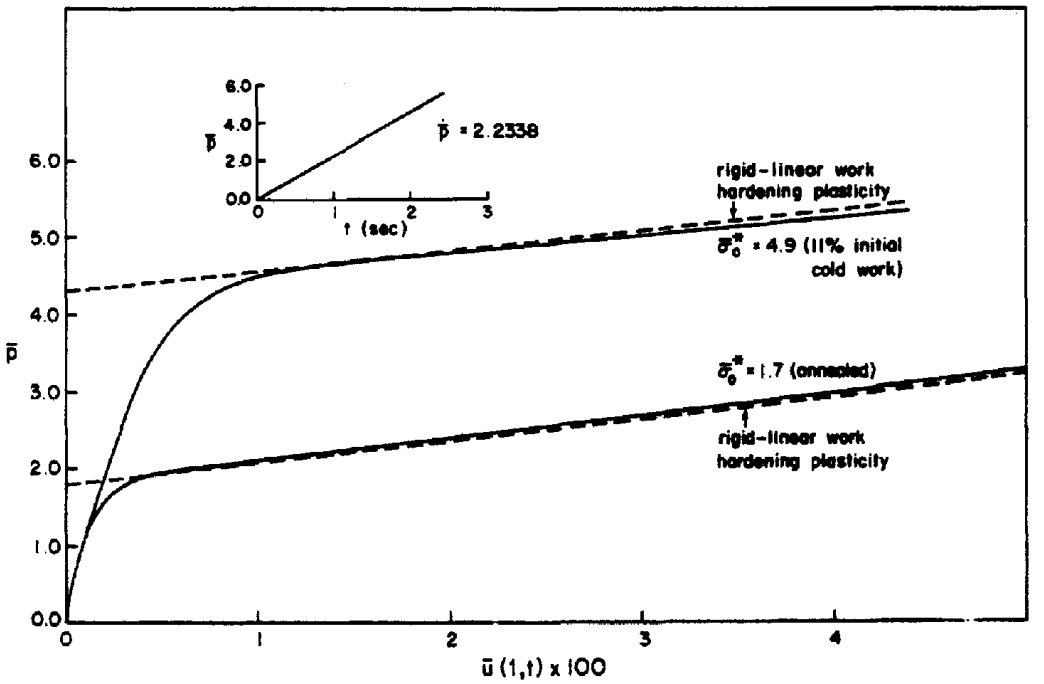

Fig. 9. Work hardening—internal pressures as functions of radial displacements at the inner wall for two values of initial hardness.

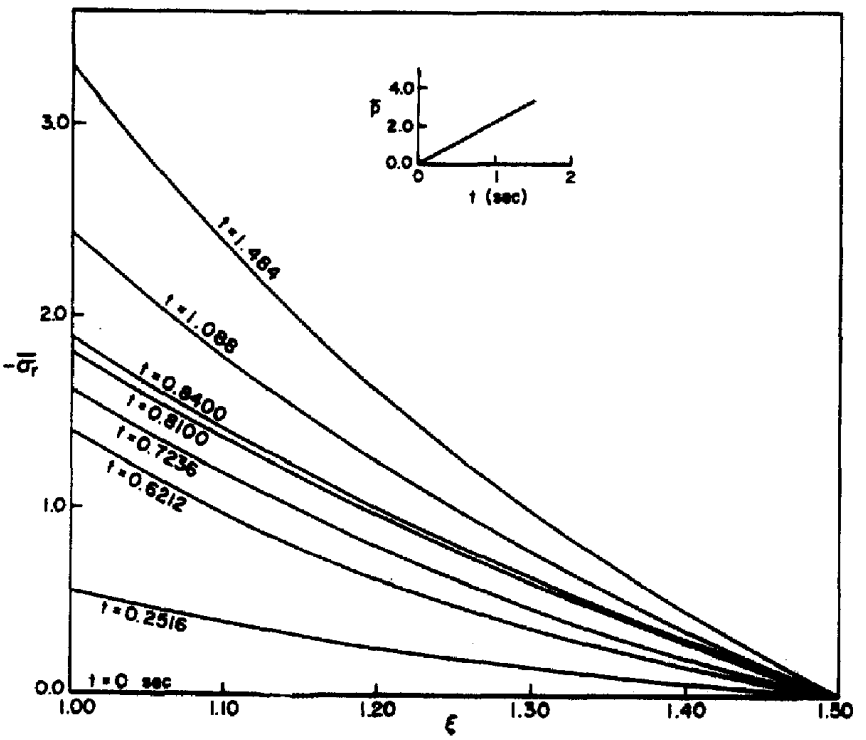

Fig. 10. Work hardening—redistribution of radial stress. $\dot{p}$ = 2.2338, $\bar{\sigma}_0^*$ = 1.7 (annealed).

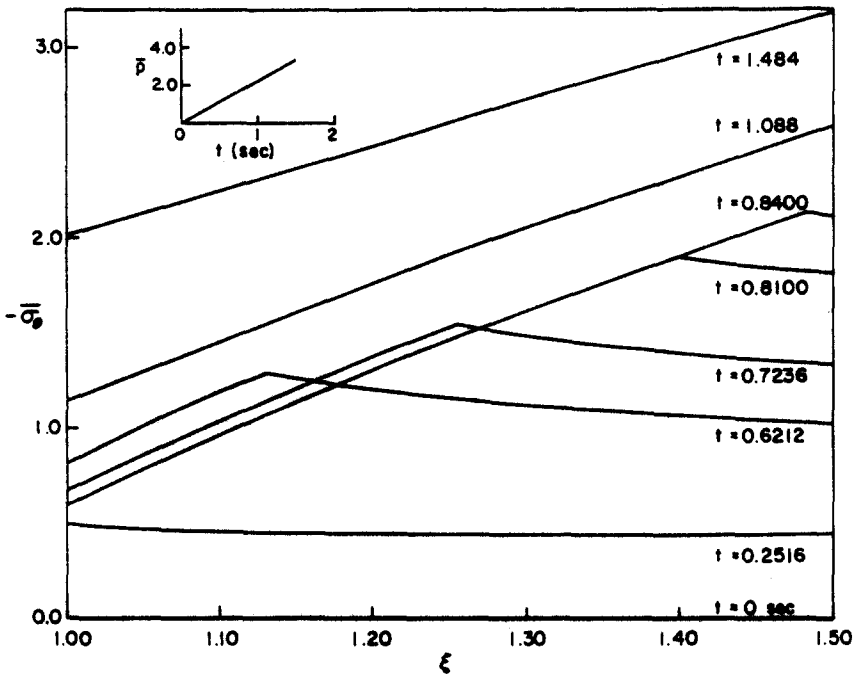

Fig. 11. Work hardening—redistribution of tangential stress. $\dot{p} = 2.2338$, $\bar{\sigma}_0^1 = 1.7$ (annealed).

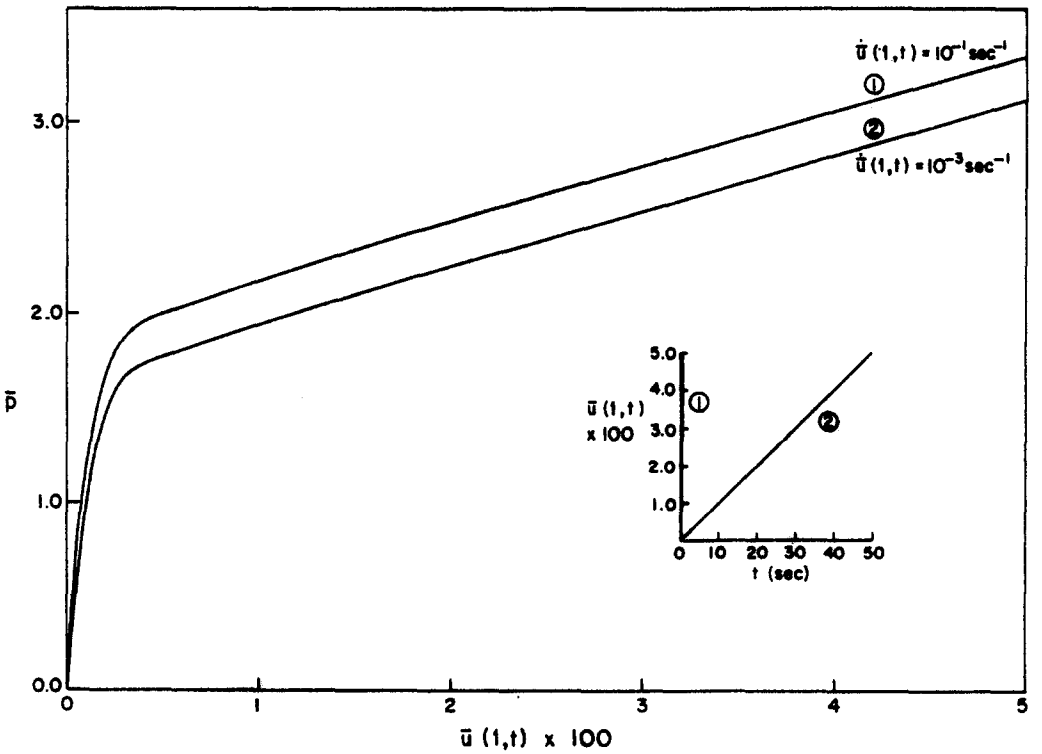

Fig. 12. Strain rate sensitivity—internal pressures as functions of radial displacements at the inner wall for two values of internal displacement rate. $\bar{\sigma}_0^1 = 1.7$ (annealed).

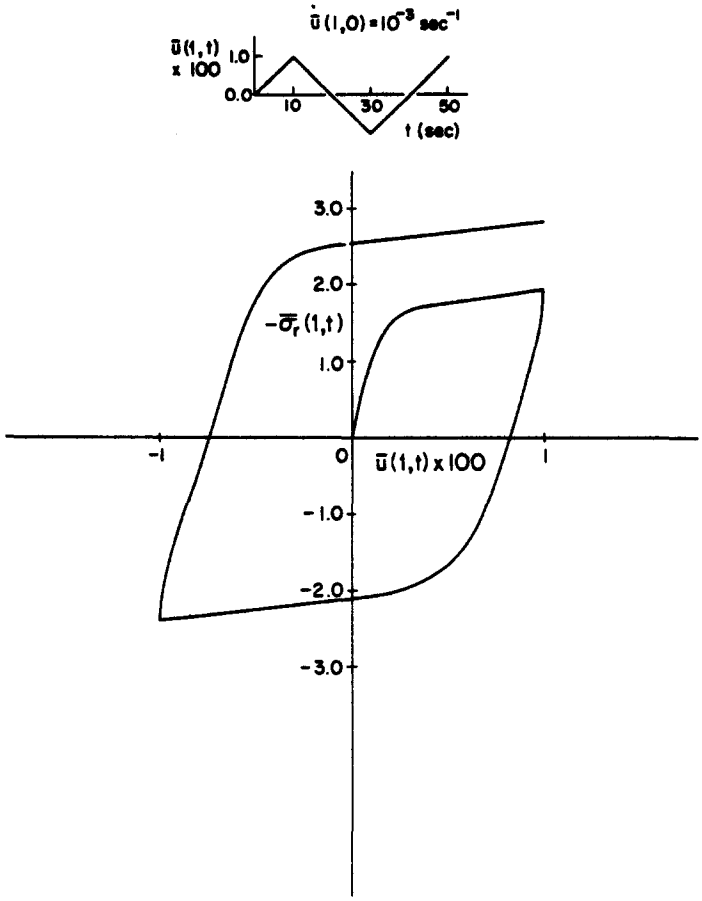

Fig. 13. Cyclic strain—radial stress as a function of radial displacement at the inner wall. $\bar{\sigma}_0^s = 1.7$ (annealed).

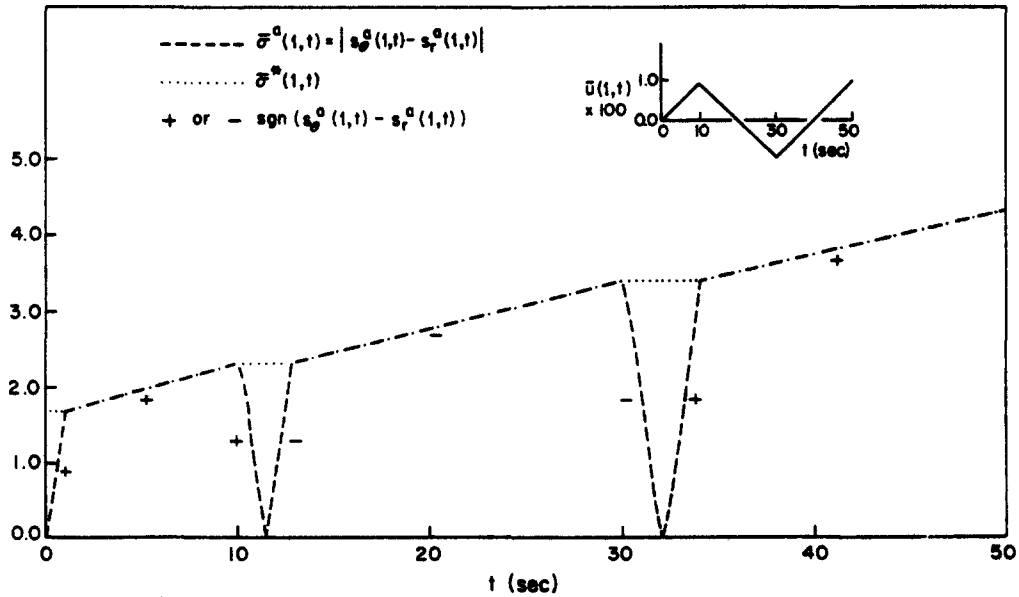

Fig. 14. Cyclic strain—hardness and anelastic stress invariant at the inner wall as functions of time. $\bar{\sigma}_0^s = 1.7$ (annealed).

increase of load and the displacement for the case of a constant internal pressure of 20 ksi is greater than that for the case where the pressure is 15 ksi for the first 3 hr and is then raised to 20 ksi.

A comparison with classical plasticity for the case of pressure increasing at a constant rate is shown in Fig. 9. The prescribed pressure rate corresponds to an initial tangential strain rate at the inner wall of 10^{-3} sec^{-1}. The yield stress and slope of the stress–strain curve for the rigid-linear work hardening plasticity model is obtained from uniaxial work hardening experiments, performed at Cornell[20]. The prescribed strain rate in these uniaxial experiments was 0.02/min. The stress–strain data was reduced to produce a plot of σ^* as a function of strain. The initial hardness of the specimen in question, σ_0^*, was the hardness value corresponding to zero strain, obtained by extrapolation. Details of this procedure, together with experimental results, are available in[20]. The correlation for two values of initial hardness is excellent. Redistribution of radial and tangential stress for this case is shown in Figs. 10 and 11. The expected propagation of the discontinuity in the slope of the tangential stress is seen in Fig. 11.

Strain rate sensitivity is shown in Fig. 12. This time the internal displacement history is prescribed. The strain rate sensitivity of 304 SS at 400°C is known to be small from experiments and this is seen in Fig. 12. The higher the strain rate, the larger is the pressure required to get the same accumulated strain.

Finally, the response to cyclic internal displacement is shown in Fig. 13. Bauschinger's effect and cyclic hardening is simulated by the theory. The nature of the stress–strain curve is qualitatively similar to that obtained from uniaxial cyclic straining experiments on metals (see for example,[22]). The behavior of the hardness and the anelastic stress invariant for this case is shown in Fig. 14. There are periods where the two are equal (analogous to tensile or compressive yielding in classical plasticity) interspersed with periods in which σ^a drops to zero and increases again.

7. CONCLUSIONS

The proposed computational scheme is very efficient for analysing the time-dependent inelastic response of structures obeying Hart's constitutive relations. Hart's model, which has been previously shown to accurately simulate quantitative uniaxial experimental results on metals for a variety of stress and strain histories, is here shown to qualitatively simulate a wide variety of experimentally observed phenomena in creep and plasticity for a structural element subjected to a multiaxial state of stress. The scalar state variable called hardness and the tensor state variable called anelastic strain is found to be adequate for representing the effect of previous deformation history on subsequent deformation behavior.

Acknowledgements—This research was supported by contract No. EY-76-S-02-2733.#000 of the Energy Research and Development Administration. Washington, D.C., with Cornell University.

REFERENCES

1. Y. N. Rabotnov, *Creep Problems in Structural Members*. North-Holland, Amsterdam (1969).
2. R. K. Penny and D. L. Marriott, *Design for Creep*. McGraw-Hill, London (1971).
3. F. K. G. Odqvist, *Mathematical Theory of Creep and Creep Rupture*. Clarendon Press, Oxford (1966).
4. E. Krempl, The interaction of rate and history-dependent effects and its significance for slow cyclic inelastic analysis at elevated temperatures. *Nuclear Engng Design* **29** (1), 125–134 (1974).
5. E. Krempl, Cyclic creep—an interpretive literature survey, *Welding Res. Council Bull.* No. 195, 63–123 (June 1974).
6. E. Krempl, On the interaction of rate and history dependence in structural metals. *Acta Mechanica*, **22** (1–2), 53–90 (1975).
7. E. W. Hart, C. Y. Li, H. Yamada and G. L. Wire, Phenomenological theory: A guide to constitutive relations and fundamental deformation properties. In *Constitutive Equations in Plasticity* (Edited by A. S. Argon). pp. 149–197. M.I.T. Press, Cambridge, Mass. (1976).
8. E. W. Hart, Constitutive relations for the non-elastic deformation of metals. *J. Engng Matls. Tech. Trans. ASME*, **98** (3), 193–202 (1976).
9. A. Miller, An inelastic constitutive model for monotonic, cyclic and creep deformation: I–Equations development and analytical procedures. *J. Engng Matls. Tech. Trans. ASME* **98** (2), 97–105 (1976).
10. A. Miller, An inelastic constitutive model for monotonic, cyclic and creep deformation: II—Application to type 304 stainless steel. *J. Engng Matls. Tech. Trans. ASME*, **98** (2), 106–113 (1976).
11. R. Lagneborg, A modified recovery-creep model and its evaluation. *Metal Sci. J.* **6**, 127–133 (July 1972).
12. D. N. Robinson, A candidate creep-recovery model for 21/4 Cr–1 Mo steel and its experimental implementation, Oak Ridge National Lab. Rep. No. *ORNL–TM–5110* (1975).

13. S. R. Bodner and Y. Partom, Constitutive equations for elastic viscoplastic strain-hardening materials, *J. Appl. Mech. Trans. ASME*, 42(2), 97E, 385–389 (June 1975).
14. V. Kumar and S. Mukherjee, Creep analysis of structures using a new equation of state type constitutive relation. *Computers and Structures*, 6, 429–437 (1976).
15. V. Kumar and S. Mukherjee, Time-dependent inelastic analysis of metallic media using constitutive relations with state variables. *Nuclear Engng Design*, 41, 27–43 (March 1977).
16. V. Kumar and S. Mukherjee, Creep analysis of metallic structures in the presence of thermal gradients using newer constitutive relations. *J. Pressure Vessel Tech., Trans. ASME*, 99J, 272–280 (May 1977).
17. S. P. Timoshenko and J. N. Goodier, *Theory of Elasticity*, 3rd Edn. McGraw-Hill, New York (1970).
18. V. Kumar, Time-dependent inelastic analysis of metallic media using constitutive relations with state variables, Ph.D. Thesis, Cornell University, Ithaca, New York (May 1977).
19. E. W. Hart, Constitutive relations for nonelastic deformation. *Nuclear Engng Design* 46, 179–185 (1978).
20. C-Y. Li, Deformation in type 304 stainless steel, third quarterly report to EPRI under Project No. RP697-1, Dept. of Materials Science and Engineering, Cornell University, Ithaca, New York (March 1977).
21. C-Y. Li, Deformation in type 304 stainless steel. *4th Qly Report to EPRI under Project No. RP*697-1. Dept. of Materials Science and Engineering, Cornell University, Ithaca, New York (June 1977).
22. J. M. Corum, Material property data for elastic-plastic-creep analyses of stiffened shear leg panel. Appendix C to *ORNL-SUB*-3754-1 by R. L. Egger, 222 (1974).